Biomicrofluidics ARTICLE pubs.aip.org/aip/bmf

An *in vitro* multi-organ microphysiological system (MPS) to investigate the gut-to-brain translocation of neurotoxins

Cite as: Biomicrofluidics **18**, 054105 (2024); doi: 10.1063/5.0200459
Submitted: 26 January 2024 · Accepted: 19 August 2024 ·
Published Online: 13 September 2024

Emily J. Jones,[1] Benjamin M. Skinner,[2] Aimee Parker,[1] Lydia R. Baldwin,[3] John Greenman,[3] Simon R. Carding,[1,4] and Simon G. P. Funnell[1,5,a)]

AFFILIATIONS

[1]Food, Microbiome and Health Research Programme, Quadram Institute, Norwich, United Kingdom
[2]School of Life Sciences, University of Essex, Colchester, United Kingdom
[3]Centre of Biomedical Sciences, Hull York Medical School, University of Hull, Hull, United Kingdom
[4]Norwich Medical School, University of East Anglia, Norwich, United Kingdom
[5]UK Health Security Agency, Salisbury, United Kingdom

[a)]**Author to whom correspondence should be addressed:** Simon.Funnell@ukhsa.gov.uk

ABSTRACT

The death of dopamine-producing neurons in the substantia nigra in the base of the brain is a defining pathological feature in the development of Parkinson's disease (PD). PD is, however, a multi-systemic disease, also affecting the peripheral nervous system and gastrointestinal tract (GIT) that interact via the gut–brain axis (GBA). Our dual-flow GIT–brain microphysiological system (MPS) was modified to investigate the gut-to-brain translocation of the neurotoxin trigger of PD, 1-methyl-4-phenylpyridinium (MPP^+), and its impact on key GIT and brain cells that contribute to the GBA. The modular GIT–brain MPS in combination with quantitative and morphometric image analysis methods reproduces cell specific neurotoxin-induced dopaminergic cytotoxicity and mitochondria-toxicity with the drug having no detrimental impact on the viability or integrity of cellular membranes of GIT-derived colonic epithelial cells. Our findings demonstrate the utility and capability of the GIT-brain MPS for measuring neuronal responses and its suitability for identifying compounds or molecules produced in the GIT that can exacerbate or protect against neuronal inflammation and cell death.

INTRODUCTION

The etiology of Parkinson's disease (PD) is not fully understood but can be attributed to both genetic and environmental factors ultimately leading to the death of dopamine-producing neurons in the substantia nigra in the base of the brain.[1] The incidence of PD globally exceeds 10×10^6 with the emotional and financial cost of patient care usually falling heavily on the partners and families of patients. Despite PD's increasing global morbidity and mortality, there is no cure or effective treatment. PD is a multi-systemic disease affecting both the peripheral nervous system and gastrointestinal tract (GIT) that collectively comprise the gut–brain axis (GBA).[2–4] Research on the GBA and its role in PD has, to date, relied on *in vivo* animal models[5,6] or static two-dimensional cell cultures, neither of which fully recapitulate human physiology.[7] Recent advances in microphysiological system (MPS) technology have enabled the development of more complex *in vitro* models to study interactions between cellular constituents of different human organ systems, including the GIT and brain.[8]

Although modeling of functional cellular barriers, such as the intestinal epithelium, endothelium, and the blood-brain-barrier (BBB) is challenging due to their complex cellular organization, MPS technology can, by combining tissue engineering and microfabrication, create more physiologically relevant models.[9,10] These MPS devices contain human cells or tissues, which, when combined with microfluidics modeling the circulatory system, can reproduce complex *in vivo* tissue-specific functions.[11,12] These

miniature devices therefore enable modeling aspects of human neurological diseases in a controlled and potentially high-throughput microenvironment.[13–16]

We have previously described the development of a dual-flow tissue perfusion MPS.[17] This modular system connects two MPS chip devices containing an inner, removable insert with a semi-permeable membrane separating intestinal epithelial or brain neuronal cells, connected via microfluidic channels. Our MPS device design has been updated for this study to be more easily assembled and user friendly for adoption by non-specialist users.

In this study, we used the modified GIT–brain MPS as a reductionist and simplified, two cell-line model to assess specific gut-to-brain drug translocation. As the brain region-specific, selective vulnerability of dopaminergic neurons is an underlying factor in PD,[18–20] we combined the differentiated human SH-SY5Y neuroblastoma cell line, which has previously been shown to be an optimal model of susceptible neurons,[21] with either the Caco2 or HT29-MTX-E12 human colonic epithelial cell lines. By incorporating the known neurotoxin trigger of PD, 1-methyl-4-phenylpyridinium (MPP^+),[22] into the GIT–brain MPS, we could assess the resulting impact on neuronal cells and, in particular, their mitochondrial and nuclear phenotypes. By combining high-throughput, quantitative, and morphometric image analysis methods, we confirmed neuronal-specific cytotoxicity and mitotoxicity *in vitro*.

The GIT–brain MPS and image analysis combination is, therefore, a promising high-throughput approach for the discovery and testing of new treatments for neurodegenerative disorders such as PD.

RESULTS

The GIT-brain MPS model

The design and fabrication of the GIT–brain MPS was based on our previous studies[17] and modified here to include an updated, more user-friendly design. The easily removable inner poly(methyl methacrylate) (PMMA) insert enables the pre-culture of cell lines off-chip prior to the assembly of the MPS. This facilitates the culture of human cell lines with differing physiological requirements, such as media composition, and enables the incorporation of cell lines such as SH-SY5Y, which require an extended culture period for differentiation into the dopaminergic neuronal cell lineage. The syringe-pump media perfusion system mimics the systemic circulation and ensures a constant supply of fresh nutrients and removal of any toxic metabolites or other cellular products.

Characterization of the GIT-brain MPS

Modular GIT and brain chip devices were connected in tandem via microfluidic tubing to create distinct channels [Fig. 1(a)]. The

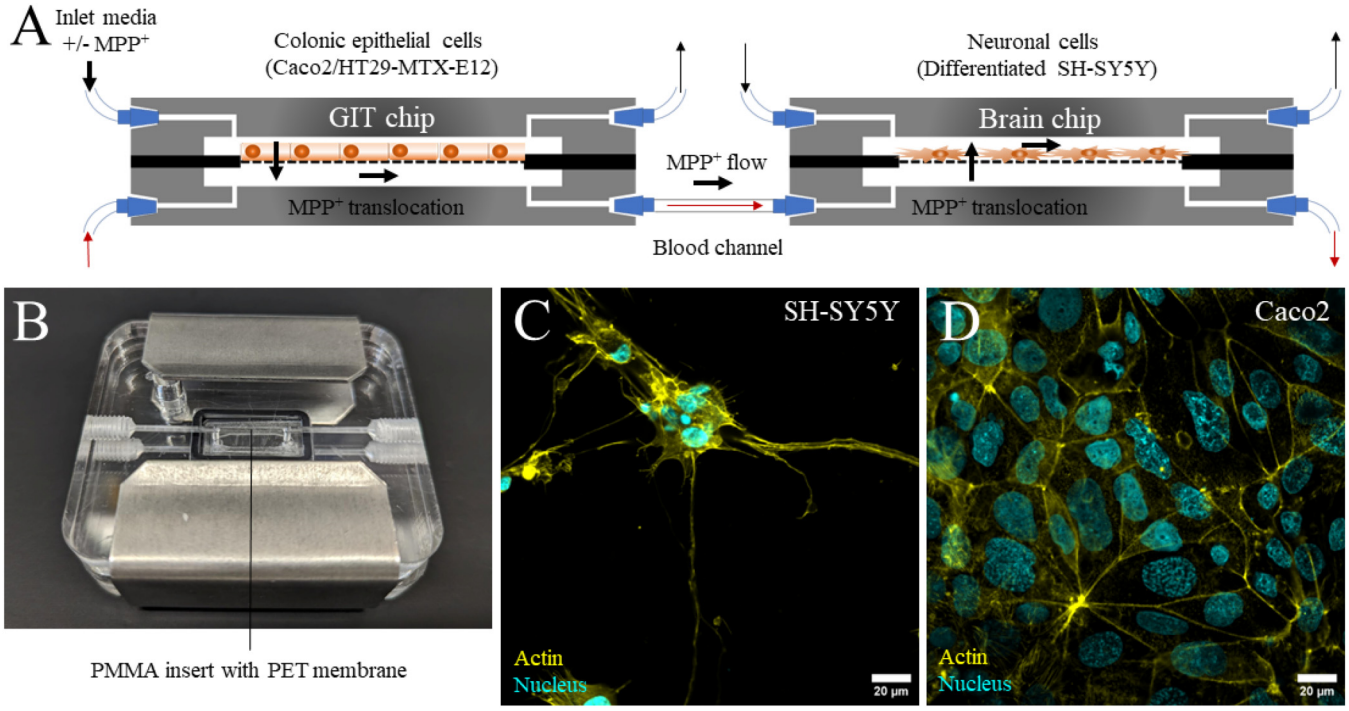

FIG. 1. GIT–brain microphysiological system (MPS). (a) Schematic of the dual-flow microfluidic chip devices connected in tandem. The arrows indicate the direction of media flow. MPP^+ is administered in media via a syringe connected to the apical inlet of the GIT chip device. The bold arrows indicate the direction of the MPP^+ flow through the connected chip devices. (b) Image of the assembled MPS device and internal PMMA insert with a 0.4 μm PET membrane for cell culture. Immunofluorescent images of (c) differentiated SH-SY5Y and (d) Caco2 cells maintained on-chip under flow for 24 h. Cells labeled with Hoechst nuclear DNA stain (cyan) and phalloidin-488 actin stain (yellow). Scale bars 20 μm.

semi-permeable membrane bonded to the removable PMMA insert facilitates the culture of human cell lines and creates two separate compartments inside each chip device with isolated dual-flow channels [Fig. 1(b)]. This mimics the distinct circulatory systems of the GIT and brain *in vivo* and replicates the selective permeability of the intestinal epithelium and endothelial BBB components of the GBA.[17] Furthermore, although the apical flow of each chip device remains distinct, the basal channels of the chip devices are connected to model the physiological communication between the GIT and brain via the circulatory system *in vivo*. By incorporating these features, the dual-flow MPS design enables the investigation both of selective translocation of MPP^+ through the apical semi-permeable cellular barriers within the GIT and brain chip devices but also translocation between the basal connecting blood channels of the devices, therefore providing a more physiologically relevant model of the *in vivo* GBA compared to traditional static 2D cell culture models. The ability of the GIT–brain MPS to maintain viable human cell cultures was confirmed following the maintenance of differentiated SH-SY5Y and Caco2 cell lines on-chip, under flow conditions, for 24 h [Figs. 1(c) and 1(d)].

MPP^+ treatment is specific for dopaminergic neuronal cells

Prior to MPP^+ treatment, the differentiation of SH-SY5Y was confirmed using the neuronal cell markers synapsin-2 (neuronal phosphoprotein), beta-III tubulin (neuronal cytoskeleton), and neurogenin-3 (neurogenesis)[23–26] [Figs. 1(a)–1(c) in the supplementary material]. Using the differentiation protocol developed by Shipley *et al.*, SH-SY5Y produced a branched network of

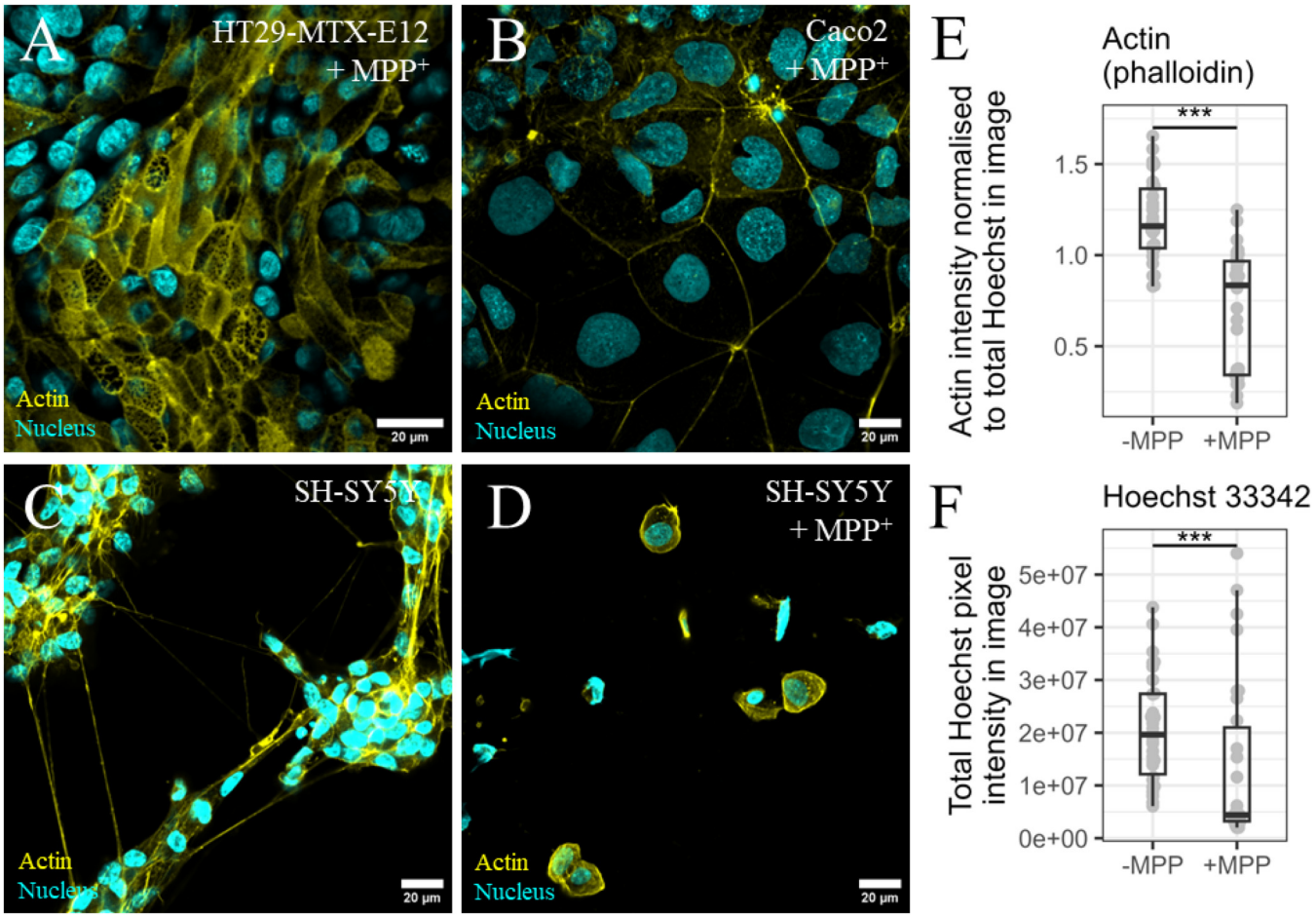

FIG. 2. MPP^+ treatment is specific for neuronal cells. Immunofluorescent images of differentiated SH-SY5Y, Caco2, and HT29-MTX-E12 cells maintained on-chip under flow conditions for 24 h. (a) Colonic epithelial HT29-MTX-E12 and (b) Caco2 cells maintained in the GIT chip devices and treated with 2000 μM of MPP^+ in the apical inlet media of the GIT chip. (c) and (d) Corresponding differentiated SH-SY5Y cells cultured in the connected brain chip. Cells labeled with Hoechst nuclear DNA stain (cyan) and phalloidin-488 actin stain (yellow). Scale bars 20 μm. (e) Quantification of actin and F. Hoechst staining of differentiated SH-SY5Y cells, either non-treated (−MPP) or treated with 2000 μM MPP^+ in the apical inlet media (+MPP). Data normalized to total Hoechst intensity per image as a control for the cell number with 30 images analyzed per treatment group. $^{***}p \leq 0.001$.

neurites with long processes connecting cell bodies, a characteristic neuronal phenotype.[27] Furthermore, differentiated SH-SY5Y were confirmed to be of dopaminergic neuronal subtype by both the cellular production of the neurotransmitter dopamine and its secretion into cell culture medium [Fig. 1(d) in the supplementary material].

To assess whether continuous perfusion via the dual-flow microfluidics altered the translocation of MPP^+ through the GIT chip device, MPP^+ was administered either to the apical side of the GIT chip device in the GIT–brain MPS or directly to static differentiated SH-SY5Y cultures in glass chamber slides. Following treatment with 2000 μM MPP^+ for 24 h, changes in the SH-SY5Y morphology associated with cell death, including cell rounding and loss of neuritic projections, were comparable both under on-chip flow conditions and static conditions (Fig. 2 in the supplementary material).

Next, the neuronal specificity for MPP^+-induced cell death was further examined in the GIT–brain MPS. Following treatment with 2000 μM MPP^+ for 24 h, both Caco2 and HT29-MTX-E12 colonic epithelial cell lines cultured in single GIT chip devices visually displayed a normal morphology with well-defined lateral junction F-actin [Figs. 2(a) and 2(b)]. In contrast, substantial loss of cell viability was observed in differentiated SH-SY5Y neuronal cells cultured in the brain chip devices [Figs. 2(c) and 2(d)]. Quantification of actin and Hoechst staining of differentiated SH-SY5Y confirmed a significant reduction in the signal [$p \leq 0.001$; Figs. 2(e) and 2(f)], indicative of cell shrinkage and detachment from the PMMA insert membrane. The total Hoechst pixel intensity was utilized here for nuclear quantification as well as to normalize actin staining. This analysis is comparable to the measurement of the cell number but is more robust as it does not rely

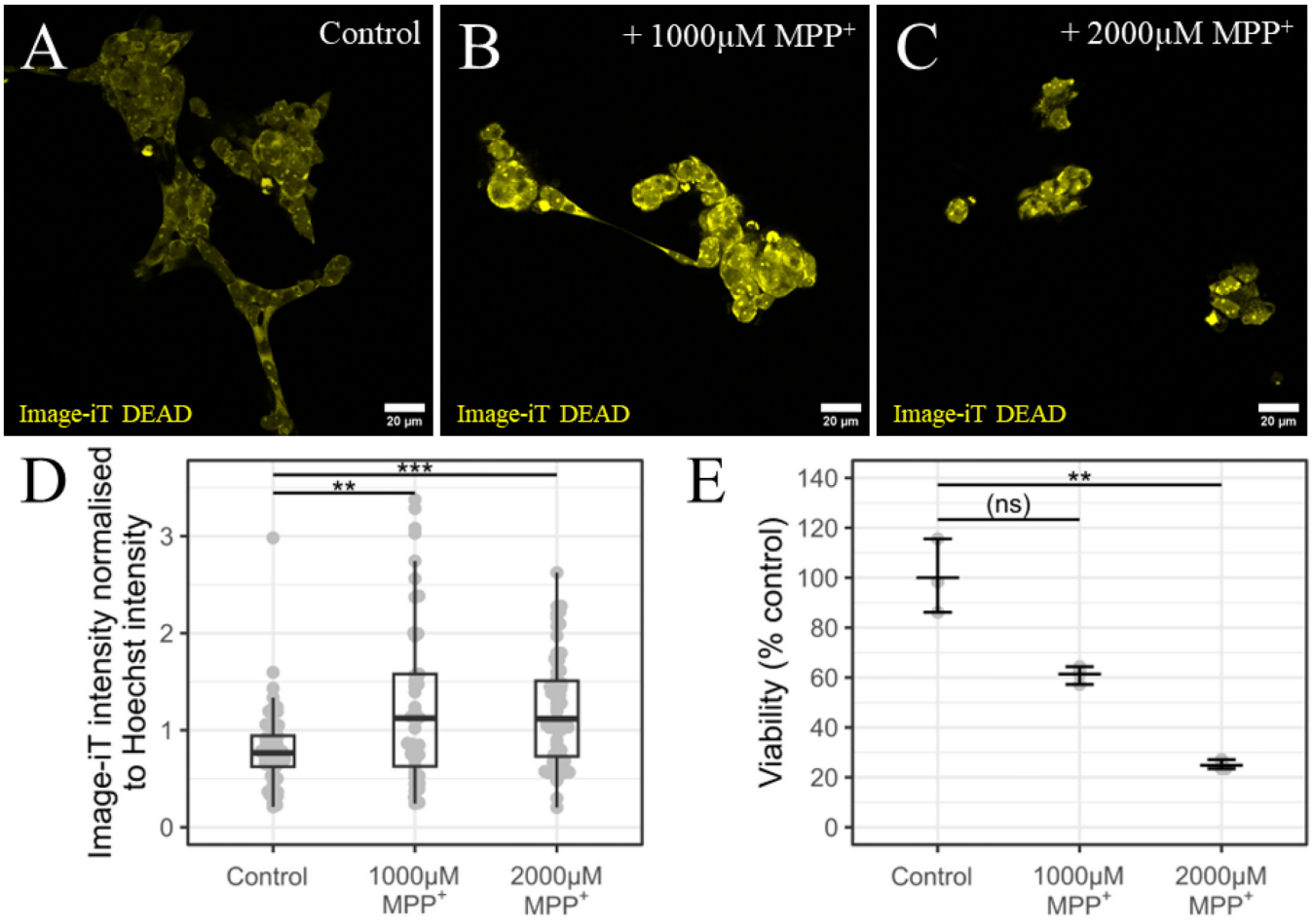

FIG. 3. Measurement of cytotoxicity in MPP^+ treated SH-SY5Y cells. Differentiated SH-SY5Y cells were cultured under static conditions and treated with MPP^+ for 24 h prior to fixation and staining with Image-iT DEAD (yellow). Immunofluorescent images of (a) non-treated cells and (b) treated with 1000 or (c) 2000 μM of MPP^+. Scale bars 20 μm. (d) Quantification of Image-iT DEAD staining from immunofluorescent images. Data normalized to the total Hoechst intensity per image as a control for the cell number. Data representative of two independent experiments with 15–45 images analyzed per treatment group. (e) Quantification of cell viability of untreated cells or treated with 1000 or 2000 μM of MPP^+. $^{**}p \leq 0.01$ and $^{***}p \leq 0.001$.

on accurate cell segmentation. Figure 3 in the supplementary material confirms that the total Hoechst pixel intensity values correlate with cell number counts ($R^2 = 0.82$; $p = 1.57 \times 10^{-23}$). This also confirms the reduction in the cell number seen in Fig. 2, although due to inaccuracies in cell segmentation leading to underestimates in cell counts, this was not significant ($p = 0.06$).

Therefore, due to the neuronal cell specificity, only the SH-SY5Y cell line was further assessed for the quantification of cytotoxicity and mitotoxicity in response to MPP^+ treatment.

Loss of neuronal cell viability in response to MPP^+ treatment

To confirm the suitability of differentiated SH-SY5Y inclusion in the GIT–brain MPS model of neurotoxin translocation, static cultures were used for high-throughput imaging and analysis. First, the level of neuronal cytotoxicity was examined using the Image-iT DEAD Green stain where increased dye uptake is associated with increased cell membrane permeability and cell death. The immunofluorescent images suggest that an increase in the signal was only observed following treatment with the lower concentration of 1000 μM MPP^+ [Figs. 3(a)–3(c)]. However, normalization using Hoechst, to account for the reduced cell number due to detachment from the PMMA insert, confirmed a significant increase in cell death following treatment with both 1000 and 2000 μM MPP^+ [Fig. 3(d)]. This finding was further confirmed using the CellTiter-Glo cytotoxicity assay. Following treatment with MPP^+ for 24 h in static chamber slides, differentiated SH-SY5Y cell viability was reduced, although this was only statistically significant for 2000 μM MPP^+ [Fig. 3(e)].

Alterations to nuclear and mitochondrial morphology

Further examination of the differentiated SH-SY5Y response to MPP^+ treatment through the visualization and quantification of nuclear and mitochondrial health staining also identified changes in the differentiated SH-SY5Y morphology associated with cell death (Figs. 4 and 5).

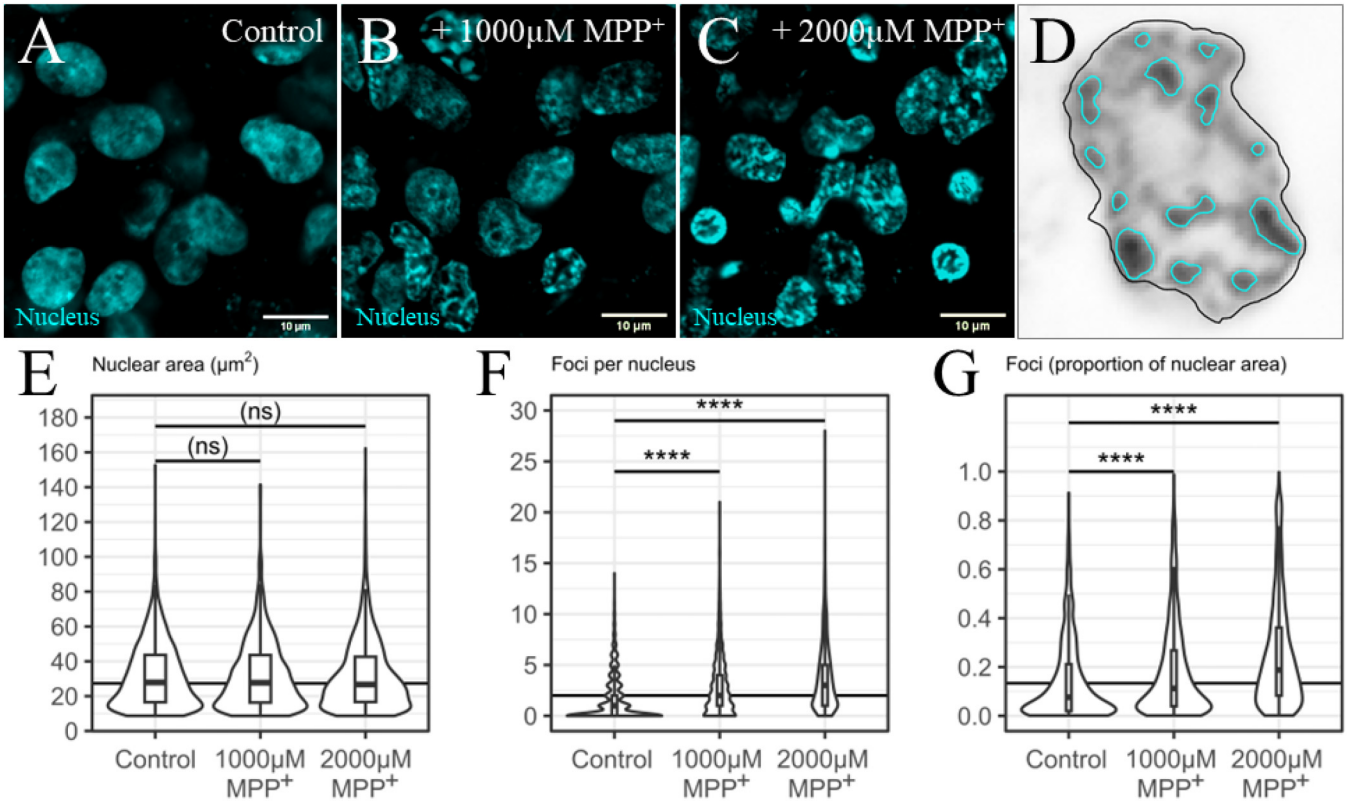

FIG. 4. Alterations to the nuclear morphology following MPP^+ treatment. Immunofluorescent images of differentiated SH-SY5Y cells maintained under static conditions in chamber slides for 24 h prior to fixation and staining with Hoechst nuclear DNA stain (cyan). Immunofluorescent images of (a) non-treated cells and (b) treated with 1000 or (c) 2000 μM of MPP^+. Scale bars 10 μm. (d) Example image of dense foci (cyan outlines) detected within a nucleus. Quantification of Hoechst staining from immunofluorescent images. Graphs depict (e) the nuclear area and (f) foci number per nucleus and G. Proportion of the nuclear area within foci. Data normalized to the total Hoechst intensity per image as a control for the cell number. Data representative of two independent experiments with 30 images analyzed per treatment group. ****$p < 0.0001$.

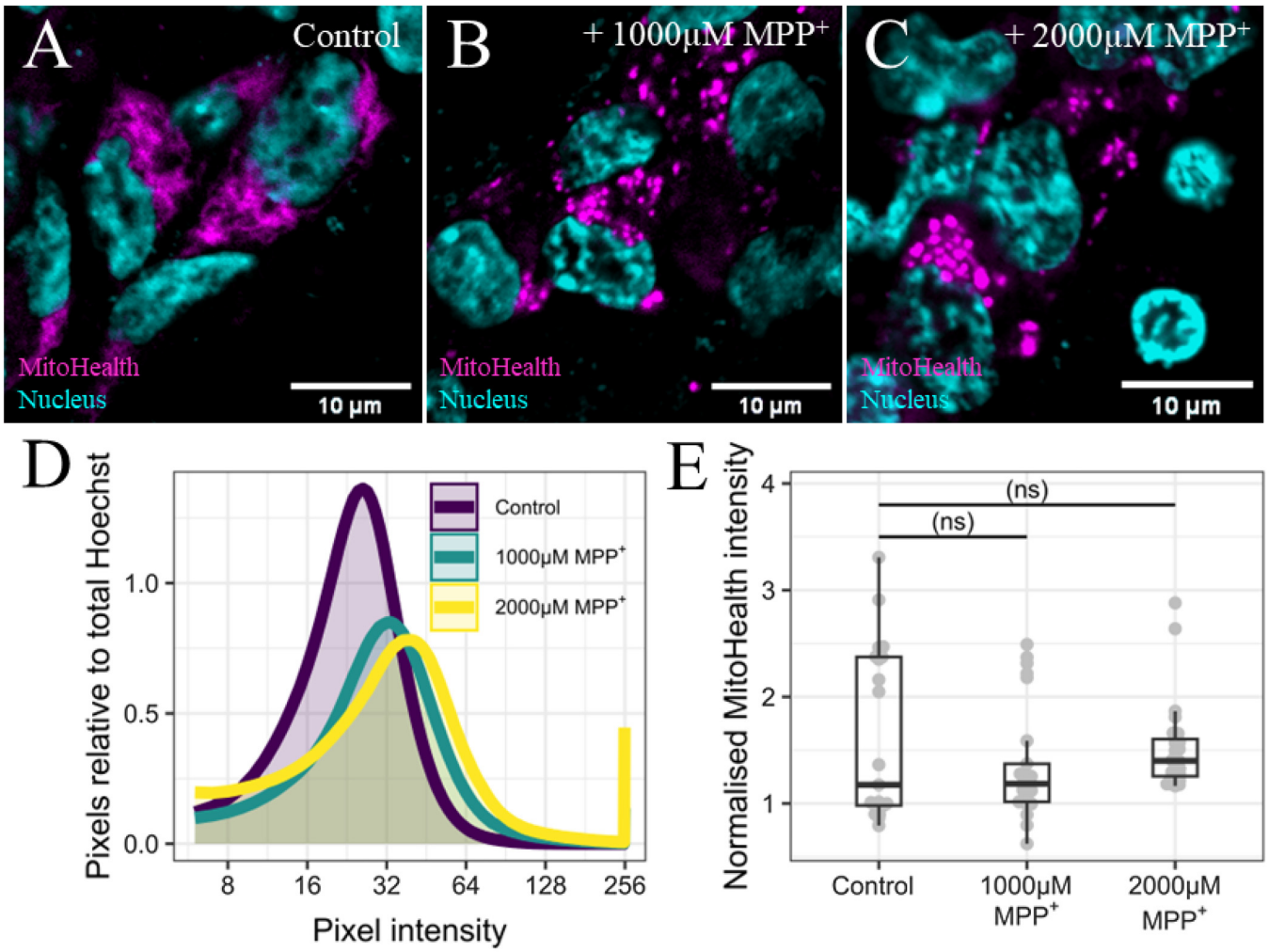

FIG. 5. Alterations to the mitochondrial morphology and membrane potential following MPP^+ treatment. Immunofluorescent images of differentiated SH-SY5Y cells maintained under static conditions in chamber slides for 24 h prior to fixation and staining with Hoechst nuclear DNA stain (cyan) and Mito Heath stain (magenta). (a) Non-treated cells and (b) treated with 1000 or (c) 2000 μM of MPP^+. Scale bars 10 μm. (d) Quantification of the Mito Health pixel number and intensity and (e) normalized intensity from immunofluorescent images of Mito Heath stain (magenta). Graphs normalized to total Hoechst intensity per image as a control for the cell number. Data representative of two independent experiments with 15–45 images analyzed per treatment group.

Although there was no observed difference in the overall size of nuclei [Figs. 4(a)–4(c) and 4(e)], there was a significant increase in both the number and proportion of nuclear area covered by dense foci [Figs. 4(d), 4(f), and 4(g)], at all concentrations of MPP^+ tested.

Furthermore, the Mito Health stain showed changes in differentiated SH-SY5Y mitochondrial functionality with MPP^+ treatment characterized by significant changes in the morphology, including mitochondrial rounding, fragmentation, and loss of connectivity compared to the non-treated control [Figs. 5(a)–5(c)]. Although no overall decrease in total pixel number was observed following MPP^+ treatment, the distribution of staining was altered [Figs. 5(d) and 5(e)]. This pattern is indicative of a loss of mitochondrial membrane potential with a corresponding increase in the Mito Health stain uptake in bright foci rather than the diffuse, connected mitochondrial staining observed in non-treated controls. Intracellular SH-SY5Y dopamine production also increased with MPP^+ treatment [Fig. 1(d) in the supplementary material].

DISCUSSION AND CONCLUSIONS

Here, we describe a simplified, physiologically relevant GIT–brain MPS to model neuronal cell death via the translocation of the neurotoxin MPP^+. The connection of the modular GIT and brain chip devices with microfluidics reflects key aspects of GBA

connectivity *in vivo* enabling us to assess the systemic effect of translocation of the neurotoxin MPP^+ across the physical cellular barrier of the colonic epithelium to determine the effect on neuronal cells.

The suitability of the differentiated SH-SY5Y cell line for inclusion in the brain chip device as a key component of the GBA was assessed by the combined quantification of cytotoxicity and mitotoxicity using static chamber slides for high-throughput image analysis. As anticipated, MPP^+ treatment caused the loss of viability specifically in differentiated SH-SY5Y dopaminergic neuronal cells,[28] while the colonic epithelial Caco2 and HT29-MTX-E12 cell lines were visually unaffected.

The differentiated SH-SY5Y cell line successfully recapitulated the MPP^+-induced changes in the morphology described in other model systems.[29–32] The loss of neuritic projections could be visualized, which is a defining feature of PD.[33] Our finding of an increase in dense nuclear foci also indicates an elevated number of transcriptionally inactive, heterochromatic foci, characteristic of the DNA damage, and cellular senescence.[34] Alterations in the neuronal mitochondrial morphology and functionality have been implicated in cellular senescence and the pathogenesis of neurological diseases.[34–36] Specifically, the disruption of mitochondrial transport leading to dynamic changes in fragmentation, fusion, and fission has become increasingly recognized as an important factor in neuronal degeneration.[37–39] Following uptake into differentiated SH-SY5Y cells, intracellular MPP^+ inhibits mitochondrial complex I of the electron transport chain, decreasing the synthesis of ATP and increasing reactive the oxygen species (ROS) production, leading to the excessive redistribution of dopamine to the cytosol,[40] which subsequently contributes to cell death.[41] Our findings of loss of mitochondrial membrane potential and significant mitochondrial fragmentation alongside increased intracellular dopamine following MPP^+ treatment were, therefore, anticipated.

Taken together, our results confirmed that differentiated SH-SY5Y are a suitable model for the quantification of neuronal-specific cell death. The image analysis software developed by the University of Essex was confirmed to support capability for the high-throughput analysis of disease modeling data, and future versions could enable analogous quantification of changes in the mitochondrial morphology.

As 3D-printing technology advances, the current GIT–brain MPS design can be adapted to include modifications including optically clear windows for long-term live microscopy-based imaging or incorporating air–liquid–interface (ALI) chip devices to induce the polarization and differentiation of ciliated epithelial cells. The apical and basal chambers of the chip devices also allow us to increase the complexity of the MPS to model the GBA. By incorporating elements of the stromal environment such as fibroblasts, pericytes, and the vascular epithelium, key elements of the GBA such as the BBB could be recapitulated. To increase functionality, constituents of the immune system and GIT microbiota could also be integrated into the GIT–brain MPS.

Inclusion of elements of the GIT microbiota or microbe-derived products will be important in future versions of the GIT–brain MPS to further study their role in the GIT-to-brain communication. Recent studies have shown that neuroinflammation and neurodegeneration are exacerbated, or even initiated, by changes in GIT microbiota composition and function,[42–44] propagated via intestinal mucosal immune and neural networks.[45,46] We have also recently shown that bacterial extracellular vesicles (BEVs) produced by commensal GIT bacteria can enter the systemic circulation and elicit anti-inflammatory responses[47] and reach the brain via transmigration through the intestinal epithelium and BBB.[48,49]

By including soluble molecules (e.g., metabolites) produced in the GIT, the GIT–brain MPS provides an ideal model system to further investigate the role of the GIT microbiota in the pathogenesis of neurological disorders such as PD. The utility of the model could also be extended to evaluating the dose, efficacy, and safety of candidate oral neurotrophic drugs to determine the impact of translocating through intestinal barrier cells on their bioavailability and activity and ability to exacerbate, or protect against, neuronal inflammation and cell death. Thus, we anticipate that our GIT–brain MPS will be widely applicable to study many pathological mechanisms of GIT–brain communication and aid in translating the findings into novel neuroprotective therapies.

MATERIALS AND METHODS

Design and fabrication of a dual-flow MPS

The MPS was designed, and devices were fabricated by the University of Hull as previously described by Baldwin *et al.*[17] [Figs. 1(a) and 1(b)]. Each device consists of two acrylic outer plates (Kingston Plastics) and a removable inner poly(methyl methacrylate) (PMMA) insert (Kingston Plastics) held in place with a rubber O-ring (RS Components Ltd.) and secured with stainless-steel clips. The PMMA insert contains a semi-permeable, 0.4 μm pore size polyethylene terephthalate (PET) membrane (SABEU) bonded to the insert using 98% chloroform (Merck). Inlet and outlet Tygon tubing (Cole-Parmer) is attached to the devices via threaded Luer connectors (IBIDI). For cell culture, PMMA inserts were sterilized in 70% EtOH for 1 h before use. The inlet tubing was connected to 20 ml sterile syringes (Becton Dickinson) containing medium and continuous perfusion carried out using a Harvard PhD 2000 syringe pump (Harvard Apparatus) at a flow rate of 2.94 μl min^{-1}. Outlet tubing was connected to 15 ml polypropylene tubes (Sarstedt) to collect effluent. The assembled MPS was maintained at 37 °C in a humidified atmosphere containing 5% CO_2.

Cell culture

The human colonic epithelial cell lines Caco-2 (ECACC 86010202) and HT29-MTX-E12 (12040401, ECACC, UK) were cultured in Eagle's Minimal Essential Medium (EMEM) with 1% non-essential amino acids (M5650; Merck) supplemented with 2 mM L-glutamine (G7513; Merck), 10% fetal bovine serum (FBS, F9665; Merck), and penicillin–streptomycin (P4333; Merck). The undifferentiated human neuroblastoma cell line SH-SY5Y (ECACC-94030304) was maintained in Eagle's Minimal Essential Medium (EMEM) with 1% non-essential amino acids (M5650; Merck) supplemented with 15% (v/v) FBS (F9665; Merck), 2 mM L-glutamine (G7513; Merck), and penicillin–streptomycin (P4333; Merck). All cells were maintained in 25 cm^2 tissue culture flasks (Sarstedt) at 37 °C in a humidified atmosphere containing 5% CO_2.

Cell culture in static slides or on-chip in the MPS

For Caco2 or HT29-MTX-E12 static cultures on 12-well removable chamber slides (IBIDI) and on-chip cultures on sterile PMMA inserts, surfaces were coated with collagen (125-50; Merck) for 2 h at 37 °C prior to seeding with cells at $1 \times 10^5/200\,\mu$l and allowing to adhere for 16 h followed by culture for a further 5 days prior to use.

SH-SY5Y neuronal cells were differentiated according to the Shipley *et al.* protocol based on the sequential removal of serum from the medium and successive RA and BDNF treatment.[27] For static and on-chip cultures, surfaces were coated with MaxGel extracellular matrix (E0282; Merck) at 37 °C for 2 h. SH-SY5Y were seeded at 1×10^5 cells in 200 μl at day 10 of the differentiation protocol and cultured for a further 8 days in differentiation media.

PMMA inserts containing cultured cells were maintained submerged in a six well plate with 2–3 ml media and subsequently assembled into the MPS [Fig. 1(b)]. The GIT and brain devices were assembled as either a single chip device or devices were connected in tandem with apical inlets connected to syringes containing cell culture media [Fig. 1(a)]. The MPS and syringe pump were maintained for 24 h at 37 °C in a humidified atmosphere containing 5% CO_2.

MPP^+ neurotoxicity assay

Caco2 and differentiated SH-SY5Y cells were cultured in static 12-well chamber slides (as above) and were either non-treated or treated with 1000 or 2000 μM of MPP^+ (Ab144783; Abcam) in cell culture media for 24 h. Under on-chip flow conditions, Caco2, HT29-MTX-E12, and differentiated SH-SY5Y cells were cultured in single or connected chip devices (as above). Following MPS assembly, the inlet medium was either non-treated or treated with 1000 or 2000 μM of MPP^+ (Ab144783; Abcam) delivered via the apical 20 ml syringe and flowed over the apical side of the membrane. This concentration range has previously been shown to be an optimal lethal dose (LD50) for differentiated SH-SY5Y.[29,50] PMMA inserts containing cells were removed from the acrylic outer plates prior to fixing and staining as below.

Immunofluorescence imaging of cell differentiation and morphology

Differentiated SH-SY5Y cells cultured in static 12-well chamber slides (as above) were stained for the presence of differentiation markers using antibodies specific for synapsin-2 (D12G5; Cell Signalling Technology), beta-III tubulin (ab201740; Abcam), and neurognin-3 (ab216885; Abcam). Cells were fixed in 4% (v/v) paraformaldehyde (PFA, 043368.9M; Thermo Fisher Scientific), washed twice with phosphate-buffered saline pH 7.4 (PBS, D8537; Merck), and then incubated with blocking buffer (1% (w/v) bovine serum albumin (BSA, 3117332001; Merck) and 10% goat-serum (G9023; Merck) in PBS at 20 °C for 1 h. Cells were then incubated with primary antibody diluted 1:200 in the blocking buffer at 4 °C for 16 h. After incubation, cells were washed three times with wash buffer (PBS with 0.05% Triton-X100, 93443; Merck) for 5 min each time on a rocking platform and then incubated at 20 °C for 1h with the secondary antibody conjugated with AlexaFluor-488 (anti-rabbit IgG, A-11008; Thermo Fisher) diluted 1:2000 in PBS. Hoechst 33342 (1:1000, H10295; Thermo Fisher Scientific) nuclear stain was incubated with cells for 30 min prior to washing with PBS and the addition of the Fluoromount-G mounting medium (0100-01; SouthernBiotech) and a high precision coverslip (IBIDI).

To visualize the cell morphology as an indicator of cell death in response to MPP^+ treatment, Caco2, HT29-MTX-E12, or differentiated SH-SY5Y cells cultured on either static 12-well chamber slides or PMMA inserts were fixed in 4% (v/v) PFA and washed twice with PBS as above. AlexaFluor-488 conjugated phalloidin (1:1000, ab176753; Abcam), for the visualization of actin filaments, and Hoechst 33342 (1:2000; H10295; Thermo Fisher Scientific) nuclear stain were incubated with cells at 20 °C for 30 min prior to washing with PBS and the addition of Fluoromount-G mounting medium (0100-01; SouthernBiotech) and a high precision coverslip (IBIDI). Prior to mounting, the semi-permeable membrane of the PMMA insert was excised and placed apical side up on a glass slide (VWR).

Slides were imaged using a Zeiss LSM880 confocal microscope equipped with 63×/1.4 oil DIC objective and Zen black software (Zeiss). Fluorescence was recorded at 405 (blue; nucleus), 488 (green; phalloidin, synapsin-2 or Neurogenin-3), and 594 nm (red; beta-III tubulin). Individual channel intensities were adjusted for appropriate visualization and set to a consistent value for comparison between treatment groups. Images were processed and pseudo-colored (magenta, yellow, and cyan) using Image J/FIJI v1.52p. Image analysis was performed using Image J/FIJI v1.52p or Nuclear Morphology Analysis 2.1.0, described in detail below.

Cell viability assay

Viability of differentiated SH-SY5Y in response to MPP^+ treatment was assessed using the CellTiter-Glo 2.0 Viability Assay (G9242; Promega) according to manufacturer's instructions. Differentiated SH-SY5Y cells were cultured on 12-well chamber slides as above and were either non-treated or treated with 1000 or 2000 μM of MPP^+ in cell culture media for 24 h. Cells including media were then incubated with CellTiter-Glo 2.0 reagent at 20 °C for 3 min on a rocking platform to induce cell lysis. Cell lysates (200 μl) were transferred to a white 96-well flat bottom plate (Nunclon delta-treated, Nunc), and luminescence was measured after 10 min using a CLARIOStar plate reader (BMG Labtech).

Dopamine ELISA

Quantification of dopamine production by differentiated SH-SY5Y cells cultured in 12-well removable chamber slides (described above) was performed using an ELISA kit (ENZO; ENZ-KIT88001). Differentiated SH-SY5Y cells were cultured on 12-well chamber slides as above and were either non-treated or treated with 1000 or 2000 μM of MPP^+ in cell culture media for 24 h. The cell medium was removed and centrifuged at 1000×g for 20 min at 4 °C, and the cells were lysed using cell lysis solution (Merck; C3228) for 15 min using a thermomixer at 20 °C and then centrifuged at 15 000× g at 4 °C. All samples were transferred to a new Eppendorf on ice, and a protease inhibitor cocktail was added at 1:100 (Merck P8340). Samples were stored at −20 °C prior to the ELISA analysis according to manufacturer's instructions.

MPP^+ mitotoxicity and cytotoxicity assay

Differentiated SH-SY5Y cells were stained with the HCS Mitochondrial Health Kit (H10295; Thermo Fisher) according to manufacturer's instructions. Differentiated SH-SY5Y cells were cultured on 12-well chamber slides (as above) and were either non-treated or treated with 1000 or 2000 μM of MPP^+ in cell culture media for 24 h.

To visualize cell staining, differentiated SH-SY5Y cells including media were incubated with cell staining solution containing Mito Health stain and Image-iT DEAD green viability stain for 30 min at 37 °C in a humidified atmosphere containing 5% CO_2. The medium was removed, and cells were incubated with fixation/counterstain solution containing 4% (v/v) PFA (043368.9M; Thermo Fisher Scientific) and Hoechst 33342 for 15 min at 20 °C. Cells were washed twice with PBS prior to the addition of the Fluoromount-G mounting medium (0100-01; SouthernBiotech) and a high precision coverslip (VWR).

Slides were imaged using a Zeiss LSM880 confocal microscope equipped with 63×/1.4 oil DIC objective and Zen black software (Zeiss). Fluorescence was recorded at 405 (blue; Hoechst), 488 (green; Image-iT DEAD), and 532 nm (red; Mito Health). Images were processed and pseudo-colored (magenta, yellow, and cyan) using Image J/FIJI v1.52p. Image analysis was performed using Image J/FIJI v1.52p (ref) or Nuclear Morphology Analysis 2.1.0, described in detail below.

Image analysis

Image analysis was performed in ImageJ v1.52p.[51] CZI images were initially processed in ImageJ to extract the pixel intensity histograms for each channel. Pixel values were exported in CSV format and analyzed in R 4.3.1.[52] Pixel intensity values per image were normalized against the Hoechst channel pixel intensities as a control for differing cell numbers between images. Total Hoechst pixel intensity values were compared to cell counts to confirm a robust correlation. Measurements and cell counts were exported for further analysis in R. The resulting normalized values were grouped by the intensity to show distributions of the weak or intense signal in the images. Pixel intensity values were compared between non-treated samples and those treated with 1000 or 2000 μM of MPP^+. For the neurotoxicity assay, the images contained actin (yellow; phalloidin) and nuclear (cyan; Hoechst 33342) channels, and for the Mito Heath assay the images contained mitochondrial health (magenta, Mito Heath), cell viability (yellow, Image-iT DEAD) and nuclear (cyan; Hoechst) channels. An example of the SH-SY5Y Mito Heath signal intensity analysis is shown in Figs. 5(d) and 5(e).

We investigated the internal nuclear structure in the Hoechst 33342 images using Nuclear Morphology Analysis 2.1.0.[53,54] Briefly, object edges were detected using the Canny edge detector and objects created via gap closing. Adjacent objects were separated by watershed transformation. Nuclei were identified as objects between 500 and 3600 pixels in area, with a circularity of 0.2–1.0. Total nuclear areas were measured. Dense staining nuclear foci were then detected by fixed thresholding, with the measurement of the foci number and area per nucleus. Variances in the texture of nuclei were examined by Grey Level Co-occurrence Matrices (GLCMs).[55] Measurements were exported for further analysis in R. An example of SH-SY5Y nucleus with detected foci is shown in Fig. 4(d).

Statistical analysis

All data are presented as individual values and mean ± standard deviation (SD) with the indicated sample sizes. GraphPad Prism 5 software (version 5.04) was used to calculate p-values for cell viability and dopamine secretion using two-way ANOVA with the Kruskal–Wallis test to analyze whether there were any significant differences between samples and Dunn's post hoc test for comparison between treatment groups. Comparisons between the cell number or pixel intensity values between treatment groups were conducted in R using Wilcoxon rank-sum tests. The coefficient of determination (R^2) between the cell number and Hoechst intensity was calculated via a linear model in R. Statistically significant differences between two mean values were considered when $^*p \leq 0.05$.

SUPPLEMENTARY MATERIAL

See the supplementary material for further data describing the morphological and physiological analysis of differentiated SH-SY5Y *in vitro*, the comparison of MPP^+ treatment under flow conditions on-chip and under static conditions, and the correlation between the total Hoechst pixel intensity and cell number.

ACKNOWLEDGMENTS

Under a collaborative agreement between the University of Essex, the University of Hull, the Quadram Institute Bioscience, and the UK Health Security Agency, funding was provided via the University of Essex's IAA Challenge Lab initiative 12288RC3302 (Public Health Challenge Lab, University of Essex via the Economic and Social Research Council) to the University of Hull and the Quadram Institute Bioscience through UKHSA. E.J.J., A.P., and S.R.C. were supported by the Biotechnology and Biological Sciences Research Council (BBSRC) Institute Strategic Programme Gut Microbes and Health BB/R012490/1 and its constituent projects under Nos. BBS/E/F/000PR10353, BBS/E/F/000PR10355, and BBS/E/F/000PR10346. B.S. was supported by the UKRI funding to the University of Essex. L.B. was funded by an Allam PhD studentship (University of Hull). The authors gratefully acknowledge the Quadram Institute Biosciences Advanced Microscopy Facility for their support and assistance in this work.

AUTHOR DECLARATIONS

Conflict of Interest

The authors have no conflicts to disclose.

Author Contributions

Emily J. Jones: Conceptualization (equal); Funding acquisition (lead); Methodology (equal); Validation (lead); Writing – original draft (lead); Writing – review & editing (supporting). **Benjamin M. Skinner:** Conceptualization (lead); Funding acquisition (supporting); Methodology (equal); Validation (supporting); Writing – original draft (lead); Writing – review & editing (supporting).

Aimee Parker: Conceptualization (supporting); Funding acquisition (supporting); Methodology (equal); Supervision (lead); Validation (supporting); Writing – review & editing (supporting). **Lydia R. Baldwin:** Conceptualization (equal); Investigation (equal); Methodology (equal); Resources (equal); Writing – review & editing (equal). **John Greenman:** Conceptualization (supporting); Funding acquisition (supporting); Methodology (supporting); Resources (lead); Writing – review & editing (supporting). **Simon R. Carding:** Conceptualization (supporting); Funding acquisition (supporting); Methodology (supporting); Resources (lead); Supervision (supporting); Writing – review & editing (supporting). **Simon G. P. Funnell:** Conceptualization (equal); Funding acquisition (equal); Project administration (equal); Resources (equal); Supervision (equal); Writing – review & editing (equal).

DATA AVAILABILITY

The data that support the findings of this study are available from the corresponding author upon reasonable request.

REFERENCES

[1]W. Dauer and S. Przedborski, "Parkinson's disease mechanisms and models," Neuron **39**, 889–909 (2003).
[2]J.-Y. Lee *et al.*, "Inflammatory gut as a pathologic and therapeutic target in Parkinson's disease," Cell Death Discovery **8**, 396 (2022).
[3]M. Hirayama *et al.*, "Gastrointestinal disorders in Parkinson's disease and other Lewy body diseases," npj Parkinson's Dis. **9**, 71 (2023).
[4]Q. Ma *et al.*, "Impact of microbiota on central nervous system and neurological diseases: The gut-brain axis," J. Neuroinflammation **16**, 53 (2019).
[5]T. Taguchi *et al.*, "Animal model for prodromal Parkinson's disease," Int. J. Mol. Sci. **21**, 1961 (2020).
[6]X. Z. Ma *et al.*, "Gut microbiota-induced CXCL1 elevation triggers early neuroinflammation in the substantia nigra of Parkinsonian mice," Acta Pharmacol. Sin. **45**, 52–65 (2024).
[7]M.-H. Kim, D. Kim, and J. H. Sung, "A gut-brain axis-on-a-chip for studying transport across epithelial and endothelial barriers," J. Ind. Eng. Chem. **101**, 126–134 (2021).
[8]O. Reiner, T. Sapir, and A. Parichha, "Using multi-organ culture systems to study Parkinson's disease," Mol. Psychiatry **26**, 725–735 (2021).
[9]C. M. Leung *et al.*, "A guide to the organ-on-a-chip," Nat. Rev. Methods Primers **2**, 33 (2022).
[10]J.-P. Frimat and R. Luttge, "The need for physiological micro-nanofluidic systems of the brain," Front. Bioeng. Biotechnol. **7**, 100 (2019).
[11]D. E. Ingber, "Human organs-on-chips for disease modelling, drug development and personalized medicine," Nat. Rev. Genet. **23**, 467–491 (2022).
[12]M. T. Raimondi, D. Albani, and C. Giordano, "An organ-on-a-chip engineered platform to study the microbiota-gut-brain axis in neurodegeneration," Trends Mol. Med. **25**, 737–740 (2019).
[13]P. M. Holloway *et al.*, "Advances in microfluidic *in vitro* systems for neurological disease modeling," J. Neurosci. Res. **99**, 1276–1307 (2021).
[14]Y. Yi *et al.*, "Central nervous system and its disease models on a chip," Trends Biotechnol. **33**, 762–776 (2015).
[15]T. Osaki *et al.*, "*In vitro* microfluidic models for neurodegenerative disorders," Adv. Healthcare Mater. **7**, 1700489 (2018).
[16]L. Miny *et al.*, "Modeling neurodegenerative diseases using *in vitro* compartmentalized microfluidic devices," Front. Bioeng. Biotechnol. **10**, 919646 (2022).
[17]L. Baldwin *et al.*, "Development of a dual-flow tissue perfusion device for modeling the gastrointestinal tract-brain axis," Biomicrofluidics **17**, 054104 (2023).
[18]R.-M. Brazdis *et al.*, "Demonstration of brain region-specific neuronal vulnerability in human iPSC-based model of familial Parkinson's disease," Hum. Mol. Genet. **29**, 1180–1191 (2020).
[19]D. Sulzer and D. J. Surmeier, "Neuronal vulnerability, pathogenesis, and Parkinson's disease," Mov. Disord. **28**, 715–724 (2013).
[20]D. J. Surmeier, "Determinants of dopaminergic neuron loss in Parkinson's disease," FEBS J. **285**, 3657–3668 (2018).
[21]J. I. Forster *et al.*, "Characterization of differentiated SH-SY5Y as neuronal screening model reveals increased oxidative vulnerability," J. Biomol. Screening **21**, 496–509 (2016).
[22]J. W. Langston, "The MPTP story," J. Parkinson's Dis. **7**(s1), S11–S19 (2017).
[23]N. J. Fiore *et al.*, "3D biocomposite culture enhances differentiation of dopamine-like neurons from SH-SY5Y cells: A model for studying Parkinson's disease phenotypes," Biomaterials **290**, 121858 (2022).
[24]L. Strother *et al.*, "Long-term culture of SH-SY5Y neuroblastoma cells in the absence of neurotrophins: A novel model of neuronal ageing," J. Neurosci. Methods **362**, 109301 (2021).
[25]E. F. Fornasiero *et al.*, "The role of synapsins in neuronal development," Cell. Mol. Life Sci. **67**, 1383–1396 (2010).
[26]J. Simon-Areces *et al.*, "Neurogenin 3 cellular and subcellular localization in the developing and adult hippocampus," J. Comp. Neurol. **518**, 1814–1824 (2010).
[27]M. M. Shipley, C. A. Mangold, and M. L. Szpara, "Differentiation of the SH-SY5Y human neuroblastoma cell line," J. Vis. Exp. **108**, e53193 (2016).
[28]J. A. Korecka *et al.*, "Phenotypic characterization of retinoic acid differentiated SH-SY5Y cells by transcriptional profiling," PLoS One **8**, e63862 (2013).
[29]K. Khwanraj *et al.*, "Differential expression of tyrosine hydroxylase protein and apoptosis-related genes in differentiated and undifferentiated SH-SY5Y neuroblastoma cells treated with MPP(.)," Neurol. Res. Int. **2015**, 734703.
[30]A. Arshad *et al.*, "TRPC1 protects dopaminergic SH-SY5Y cells from MPP+, salsolinol, and N-methyl-(R)-salsolinol-induced cytotoxicity," Acta Biochim. Biophys. Sin. **46**, 22–30 (2013).
[31]X. Wang *et al.*, "DLP1-dependent mitochondrial fragmentation mediates 1--methyl-4-phenylpyridinium toxicity in neurons: Implications for Parkinson's disease," Aging Cell **10**, 807–823 (2011).
[32]M. Zilocchi *et al.*, "Mitochondrial alterations in Parkinson's disease human samples and cellular models," Neurochem. Int. **118**, 61–72 (2018).
[33]O. A. Levy, C. Malagelada, and L. A. Greene, "Cell death pathways in Parkinson's disease: Proximal triggers, distal effectors, and final steps," Apoptosis **14**, 478–500 (2009).
[34]M. Kritsilis *et al.*, "Ageing, cellular senescence and neurodegenerative disease," Int. J. Mol. Sci. **19**, 2937 (2018).
[35]D. Lu *et al.*, "Mitochondrial transport in neurons and evidence for its involvement in acute neurological disorders," Front. Neurosci. **17**, 1268883 (2023).
[36]D. Trinh *et al.*, "The multi-faceted role of mitochondria in the pathology of Parkinson's disease," J. Neurochem. **156**, 715–752 (2021).
[37]A. B. Knott *et al.*, "Mitochondrial fragmentation in neurodegeneration," Nat. Rev. Neurosci. **9**, 505–518 (2008).
[38]M. Zhu, W. Li, and C. Lu, "Role of alpha-synuclein protein levels in mitochondrial morphology and cell survival in cell lines," PLoS One **7**, e36377 (2012).
[39]S. Moradi Vastegani *et al.*, "Mitochondrial dysfunction and Parkinson's disease pathogenesis and therapeutic strategies," Neurochem. Res. **48**, 2285–2308 (2023).
[40]H. Xicoy, B. Wieringa, and G. J. M. Martens, "The SH-SY5Y cell line in Parkinson's disease research: A systematic review," Mol. Neurodegener. **12**, 10 (2017).
[41]J. Lotharius and K. L. O'Malley, "The Parkinsonism-inducing drug 1--methyl-4-phenylpyridinium triggers intracellular dopamine oxidation. A novel mechanism of toxicity," J. Biol. Chem. **275**, 38581–38588 (2000).
[42]S. Romano *et al.*, "Meta-analysis of the Parkinson's disease gut microbiome suggests alterations linked to intestinal inflammation," npj Parkinson's Dis. **7**, 27 (2021).

[43]G. Saxami *et al.*, "The gut–organ axis within the human body: Gut dysbiosis and the role of prebiotics," Life **13**, 2023 (2023).
[44]J. Harsanyiova, T. Buday, and A. Kralova Trancikova, "Parkinson's disease and the gut: Future perspectives for early diagnosis," Front. Neurosci. **14**, 626 (2020).
[45]C. Pellegrini *et al.*, "Interplay among gut microbiota, intestinal mucosal barrier and enteric neuro-immune system: A common path to neurodegenerative diseases?," Acta Neuropathol. **136**, 345–361 (2018).
[46]J. F. Cryan and T. G. Dinan, "Mind-altering microorganisms: The impact of the gut microbiota on brain and behaviour," Nat. Rev. Neurosci. **13**, 701–712 (2012).
[47]S. Fonseca *et al.*, "Extracellular vesicles produced by the human gut commensal bacterium bacteroides thetaiotaomicron elicit anti-inflammatory responses from innate immune cells," Front. Microbiol. **13**, 1050271 (2022).
[48]A. Modasia *et al.*, "Regulation of enteroendocrine cell networks by the major human gut symbiont bacteroides thetaiotaomicron," Front. Microbiol. **11**, 575595 (2020).
[49]R. Stentz *et al.*, "Fantastic voyage: The journey of intestinal microbiota-derived microvesicles through the body," Biochem. Soc. Trans. **46**, 1021–1027 (2018).
[50]P. Chanthammachat and P. Dharmasaroja, "Metformin restores the mitochondrial membrane potentials in association with a reduction in TIMM23 and NDUFS3 in MPP+-induced neurotoxicity in SH-SY5Y cells," EXCLI J. **18**, 812–823 (2019).
[51]C. A. Schneider, W. S. Rasband, and K. W. Eliceiri, "NIH Image to ImageJ: 25 years of image analysis," Nat. Methods **9**, 671–675 (2012).
[52]Team, R.C., *R: A Language and Environment for Statistical Computing* (2022).
[53]B. M. Skinner, "Nuclear morphology analysis 2.0.0 improved image analysis software for measuring nuclear shape," J. Open Source Software **7**, 4767 (2022).
[54]B. M. Skinner *et al.*, "A high-throughput method for unbiased quantitation and categorization of nuclear morphology," Biol. Reprod. **100**, 1250–1260 (2019).
[55]R. M. Haralick, K. Shanmugam, and I. Dinstein, "Textural features for image classification," IEEE Trans. Syst. Man Cybern. **3**, 610–621 (1973).